ADVANCED MATERIALS
www.advmat.de

The Electrical and Optical Properties of Organometal Halide Perovskites Relevant to Optoelectronic Performance

*Valerio Adinolfi, Wei Peng, Grant Walters, Osman M. Bakr, and Edward H. Sargent**

Organometal halide perovskites are under intense study for use in optoelectronics. Methylammonium and formamidinium lead iodide show impressive performance as photovoltaic materials; a premise that has spurred investigations into light-emitting devices and photodetectors. Herein, the optical and electrical material properties of organometal halide perovskites are reviewed. An overview is given on how the material composition and morphology are tied to these properties, and how these properties ultimately affect device performance. Material attributes and techniques used to estimate them are analyzed for different perovskite materials, with a particular focus on the bandgap, mobility, diffusion length, carrier lifetime, and trap-state density.

1. Introduction

Perovskite materials have increasingly attracted attention as solution-processed semiconductors for photovoltaics.[1] Solar cells remain a key emphasis of this field. Remarkable results have been achieved in improving the power conversion efficiency of perovskite solar cells: they have now crossed the 22% certified milestone.[2]

Recently, research on perovskites has diversified beyond solar cells, with a variety of different devices garnering interest. As light absorbers, these materials are also used in light detectors.[3–7] As light-emitting materials, perovskites are used to fabricate light-emitting diodes (LEDs) and optically pumped lasers.[8–10] The materials synthesis has also evolved and, as a result, a variety of different semiconductors and film morphologies can now be obtained. Along with the traditional thin film form, a single-crystal version of these materials has been produced and used for applications.[11–17]

Given the increasing variety of materials and the sophistication of optoelectronic applications, gaining a deeper and more systematic quantitative picture of the optical and electrical properties of perovskites is important. Knowing the fundamental properties of these materials is crucial for the design of advanced applications and the development of accurate analytical models and simulations.

Dr. V. Adinolfi, G. Walters, Prof. E. H. Sargent
Department of Electrical and Computer Engineering
University of Toronto
10 King's College Road, Toronto, Ontario M5S 3G4, Canada
E-mail: ted.sargent@utoronto.ca
Dr. W. Peng, Prof. O. M. Bakr
Division of Physical Sciences and Engineering
KAUST Catalysis Center and KAUST Solar Center
King Abdullah University of Science and Technology (KAUST)
Thuwal 23955-6900, Saudi Arabia

DOI: 10.1002/adma.201700764

Here, we review the optical and electrical properties of perovskites. We place particular emphasis on methylammonium (MA) and formamidinium (FA) lead halides. We compare the relevant material properties (mobility, diffusion length, lifetime, optical bandgap) for different materials and morphologies, and analyze different methods for the measurement of physical properties, highlighting benefits, limitations, and the range of validity of each. We pay particular attention to the characterization of electronic trap state densities, a key quantity for perovskite materials. We then correlate material properties with applications, defining the desirable qualities—and therefore the materials and morphologies—that are crucial for specific devices.

1.1. Perovskites for Optoelectronics

Perovskites form a large and complex material system that offers a wide set of material properties, morphologies, and syntheses. Lead halide based materials benefit from electronic properties (high mobility and low trap density as detailed herein) and spectral tunability. Referring to the canonical perovskite structure ABX_3, we focus on materials in which A, the cation, can be either MA ($CH_3NH_3^+$) or FA ($H_2N{-}CH{=}NH_2^+$); B is lead (Pb^{2+}); and X is a halide (I^-, Br^-, or Cl^-).

A major element of flexibility in this materials set is provided by the halide: by creating halide mixtures[18] (e.g. $I_{3-x}Cl_x$), one can finely tune the optical and electrical bandgap. In optoelectronic applications, this enables engineering of the emitted and absorbed wavelengths. The bandgap of lead halide perovskites can be tuned over a range spanning the near-infrared to near-ultraviolet wavelengths.

These materials have been synthesized in many different fashions and morphologies. Early thin films were produced using solution processing and thermal evaporation techniques. These films initially presented an average grain size on the nanometer scale; however, with the latest advances, today's films can show an average grain size well above 1 μm.[19] The morphology plays a major role in the performance of the perovskite film, a fact that means that mobility, trap density, lifetime, etc., must always be contextualized and compared with fabrication method and resultant morphology in mind.

Recently, methods for the synthesis of single-crystal lead halide perovskites have been developed.[16] The crystalline quality makes these materials ideal for fundamental characterization of the bulk material; electronic properties are not

degraded by morphological disorder and grain boundaries. They possess superior optoelectronic properties compared to thin-film morphologies.

The lead halide perovskite material system has been used to produce an impressive variety and quality of optoelectronic devices. Thin films were the first form of these perovskites to be developed and can be used for large-area deposition on conventional and flexible substrates.[20] Single crystals are at an initial development stage. The size and shape of these materials is still not fully controlled, and so today this limits their application. Nevertheless, high-performance light detectors have been fabricated from single crystals.[6] Perovskite nanocrystals are also at an early stage of development, where they have been used for light-emitting devices that leverage the bandgap tunability and the increased binding energy of the exciton, favoring radiative recombination.

Next we turn to summarizing the materials optoelectronic properties of lead halide perovskites. The methods used to characterize these materials, the measurement challenges specific to perovskites, and the fundamental properties related to materials morphology and composition are analyzed. We then assess the roadmap to material properties that enable commercial applications.

2. Optical Properties

2.1. Material Attributes

The absorption edge reports the optical bandgap; the steepness of the absorption onset and the presence of a tail below the absorption edge indicate the quality of the material, related to the presence of imperfections and defects within the material. A pure material will present a steep onset and no tail.[21] Additionally, the spectral absorption can offer insights into the nature of photogeneration: excitonic materials often exhibit a characteristic exciton peak that distinguishes them from band-like materials. The perovskite solids reviewed herein exhibit a direct bandgap. This feature enables high absorption crucial for optoelectronic applications such as photovoltaics.

The photoluminescence (PL) peak, another important attribute, gives information about the optical bandgap. The absorption edge and the PL peak can differ by several nanometers via Stokes and anti-Stokes shifts. The extent of the shift suggests structural disorder.[22] The spectral spread of the PL peak, characterized by its full width at half maximum, is also useful as an indicator of the densities of traps and morphological disorder; a broad PL spectrum (or the presence of tails) suggests the presence of optically active in-gap states. These features are frequently observed in disordered materials (polycrystalline and amorphous). The quantum yield (QY) of the PL, an attribute characterizing the efficiency of the radiative recombination of photocarriers, can provide information about the defects responsible for nonradiative recombination.

The evolution of PL intensity with time, i.e., the PL decay dynamics, gives a measure of the lifetime of photocarriers within the semiconductor. Typically it is fit using single or multiple exponential decay functions. The types of fitting functions are justified by the different recombination pathways;[23,24] while the PL decay is commonly fit with a single exponential decay for most thin films, a biexponential model is required to describe the PL decay in perovskite single crystals.[16] The two components are often proposed to result from a spatial distribution of defects: the surface may exhibit fast decay as a result of surface degradation and dangling bonds; and the

Valerio Adinolfi holds a B.Sc. and M.A.Sc. from the Università degli Studi Roma Tre, Rome, Italy. He finalized his M.Sc. studies at the University of Toronto, Canada, under the supervision of Prof. S. Voinigescu and G. Conte, with a thesis on modeling high-speed SiGe HBTs. He completed his Ph.D. at the University of Toronto in the Sargent group, studying the electrical properties of solution-processed semiconductors and developing optoelectronic devices. His thesis was on solution-processed light detectors. He is currently a postdoctoral researcher at the University of California, Berkeley, in Prof. Ali Javey's group.

Osman M. Bakr holds a B.Sc. in Materials Science and Engineering from MIT (2003) as well as a M.S. and a Ph.D. in Applied Physics from Harvard University (2009). He is currently an Associate Professor of Materials Science and Engineering at KAUST, Saudi Arabia. His research group focuses on the study of hybrid organic–inorganic nanoparticles and materials; particularly, advancing their synthesis and self-assembly for applications in photovoltaics and optoelectronics.

Edward H. Sargent received a B.Sc.Eng. in Engineering Physics from Queen's University in 1995 and his Ph.D. in Electrical and Computer Engineering from the University of Toronto in 1998. He is University Professor in the Edward S. Rogers Department of Electrical and Computer Engineering at the University of Toronto; Canada Research Chair in Nanotechnology; and serves as Vice President, International at the University of Toronto.

bulk shows a longer decay that benefits from the lower trap density in the bulk of the semiconductor.

Two key material parameters when considering the photonic aspects of optoelectronic devices are the refractive index and the extinction coefficient, which together make up the complex dielectric function. For solar cells, this quantity is essential for understanding and optimizing the cavity electro-optics of the device. The dielectric function is an input for modeling transmission and reflection at interfaces throughout the cell, and, ultimately, absorption by the active material. Models of the optical field distribution within the cell provide the spectrally resolved position-dependent photoexcitation profile and can be used to estimate the spectral response of the cell. They can provide engineering guidelines in the choice of layer thicknesses and compositions. These models can also be used in the design of tandem solar cells and for estimating the dependence of cell performance on the angle of incident sunlight. Knowledge of the dielectric function of perovskites is important for optoelectronic devices beyond solar cells, such as for engineering resonators for perovskite lasers, and designing the spectral response of photodetectors.

2.2. Techniques

Table 1 lists techniques to characterize a material's optical properties. The absorption spectrum of a material is readily acquired using a commercial spectrometer. To obtain an accurate absorption spectrum of solid samples, an integrating sphere is required to collect both the transmitted and reflected light, so as to deduce the absorbed light. The absorption edge can then be determined from the linear region that follows the absorption onset. By plotting the square of the absorption as a function of the photon energy, one may determine the optical bandgap via the Tauc method. To gain knowledge of the steepness of the absorption onset (the investigation of the absorption tail), a precise measurement of the sub-bandgap absorption (low absorption) is required. Photothermal deflection spectroscopy (PDS) and Fourier-transform photocurrent spectroscopy (FTPS) provide the needed sensitivities down to 10^{-4} and 10^{-6}, respectively.[25]

Techniques used to measure PL are described in Table 1. PLQY is measured using similar instrumentation as for static PL measurement; in this case an integrating sphere allows one to account for the anisotropic emission and scattering of the sample. The dependence of the PLQY on the intensity of the incident light should also be considered. As the intensity increases, traps within the perovskite gradually fill. Eventually, as fewer traps become available, bimolecular recombination dominates and the QY saturates. Transient PL can be measured with the aid of a time-correlated single photon counting (TCSPC) system or a streak-camera.

The refractive index and extinction coefficient are primarily measured through spectroscopic ellipsometry techniques, where changes in the polarization state of light reflected from the material is recorded as a function of the incident angle and wavelength. The data can be fit with a Kramers–Kronig consistent oscillator model that also accounts for multiple reflections within the thin films of known thickness. Important considerations for perovskite materials are the surface roughness and the presence of any voids in films. These factors can be incorporated into the models through effective medium approximations and estimates obtained through atomic force microscopy or scanning electron microscopy. Near-normal incidence reflectance and transmission measurements, which are complimentary to ellipsometry techniques, can add to the spectral evaluation of the dielectric function. Using the complex dielectric function, the transfer matrix method can be applied to model the cavity behavior of the optoelectronic device.

2.3. Materials

Hybrid perovskites semiconductors are direct-bandgap semiconductors. The direct transition produces large absorption coefficients on the order of 10^4–10^5 cm^{-1}. Detailed studies of the sub-bandgap absorption of $MAPbI_3$ thin films using PDS and FTPS revealed a clear, sharp absorption edge (i.e., no absorption tail), demonstrating the high quality of solution-processed perovskite films. The composition and morphology dramatically affect the optical properties of perovskites. **Figure 1** reports the absorption edge and the PL peak wavelength for lead halide perovskites of different compositions and morphologies. The sizes of the halides are a determining factor of the size of the unit cell and so further affect the electronic band structure. It was found that the large iodine cation expands the perovskite unit cell to produce materials showing a small bandgap and a corresponding absorption edge close to 800 nm for MA-based perovskites.[26–31] Substituting iodine with the smaller bromine shifts the absorption edge to ≈550 nm.[32,33] Substituting bromine for chlorine then further decreases the absorption edge to ≈420 nm.[34] Replacing MA with FA can red-shift the absorption onset ≈40 nm, which makes $FAPbI_3$ even more suitable for solar cells. This is one of the reasons for $FAPbI_3$'s use in most of today's highest-performance perovskite solar cells.

The physical mechanism behind the bandgap control, and so the absorption and emission, of perovskites through tuning the halide stoichiometry lies in their electronic band composition. Density functional theory (DFT) calculations revealed that the projected density of states (DOS) in the upper valence bands of methylammonium lead halide perovskites are mostly formed from halide p states with some admixture of lead s states, while those of the conduction bands consist of mainly lead states. As a result, the halide composition has a deep impact on the valence band of perovskite electronic structures, as demonstrated both from calculations and experiments.[35,36] In contrast, the replacement of MA with FA makes only a slight change to the bandgap, as expected. Furthermore, the unoccupied p states of lead contribute to a high DOS in the lower part of the conduction band of perovskites. Therefore, the direct p–p transitions in perovskites results in a stronger optical absorption than other absorbers in current high-efficiency thin film solar cells such as GaAs and CdTe.[25,37] Despite the possibility of continuously tuning the absorption and emission of perovskites by producing halide mixtures, several research groups reported light-induced phase separation in mixed-halide perovskites. This phenomenon of materials instability is detrimental for applications, and has not yet been completely understood.

Table 1. Optical properties.

Property	Absorption		PL			Dielectric constant
	Absorption spectrum	Sub-bandgap absorption	PL spectrum	PLQY	PL decay	Refractive index and extinction
Techniques	Commercial spectrometers consisting of a light source, a monochromator, a sample chamber (for solid samples, this should be an integrating sphere), and a photodetector. Transmission of light through the sample is measured as a function of wavelength.	PDS: an indirect method to extract the absorption via photoabsorption-induced thermal state changes; FTPS: from the measurement of photocurrent based on Fourier transform, the absorption is extracted.	Commercial spectrometers consisting of a monochromatized light source for photoexcitation, a spectrometer to separate the spectrum of the emitted light spatially, and a photodetector.	Similar to PL measurement instruments, but here an integrating sphere is used. Incident and emitted light intensities are recorded to determine the conversion efficiency.	TCSPC: consist of a pulsed laser system synchronized with the detector. Emitted photons are detected temporally relative to the exciting pulse and a histogram of emission events is generated for different delay times. Streak-cameras: work by translating temporally varying pulses of emitted light to spatially varying pulses. The emitted light pulses impinge on a photocathode to generate electrons, which can then be spatially modulated with an electric field to form a streak image on a detector screen.	Spectroscopic ellipsometry measures changes in polarized light incident on the material thin films at varying incidence angles and wavelengths. Complemented with reflectance and transmission measurements.

Figure 1 shows that for every material composition there is a wide spread in the values for the absorption edge and the PL emission peak. This spread is attributable mainly to variations in the material morphology and crystallinity. It has been observed that perovskite single crystals exhibit absorption edges and PL peaks shifted to red wavelengths when compared to the thin film counterparts.[6,16,17,38–43] The origin of this difference is still not completely understood.

The dielectric properties of perovskites have been measured by several groups,[44–48] some of which have then used the information to model the cavity characteristics of solar cells.[44,47] The measured extinction coefficients, as expected, follow the features of the absorption spectra, and the measured refractive indices of thin films of $MAPbI_3$ and $MABr_3$ are, respectively, ≈2.5[44,45,47,48] and ≈2.0[46] at optical wavelengths in the transparency regime. The refractive indices of single crystals has also been observed to be greater for single crystals than for thin films.[46] Cavity modeling of solar cells has produced photoexcitation profiles that show a highly absorbing Beer–Lambert regime at short wavelengths and a thin film interference regime at longer wavelengths, suggesting that the spectral response of the cells at long wavelengths is greatly dependent upon the active layer thickness.[44] The optimal thickness for the active layer is predicted to be ≈300 nm,[44,47] a prediction that is widely reflected experimentally in the literature for the best performing devices.

3. Electrical Properties

3.1. Material Attributes

Knowledge of a material's electrical properties, such as charge carrier mobilities, diffusion lengths, and lifetimes, is crucial for fabricating optoelectronic devices as well as for developing robust models for device simulations.

The electrical mobility, μ, describes the ability of a charge carrier (either electrons, μ_e, or holes, μ_h) to move within a semiconductor under an applied field. Mobility is important for applications such as field effect transistors (FETs) and photodetectors, where a drift electrical transport mechanism is desirable in order to obtain a fast response time.[49]

Another important quality describing charge transport is the diffusion length. Also in this case, the figure distinguishes between electrons (L_e) and holes (L_h). This quantity describes the motion of charges by diffusion from regions of high carrier population in the semiconductor to areas with lower populations. The diffusion lengths are crucial performance factors in optolectronics where light excitation produces local excesses of charge. The diffusion length is one of the fundamental parameters governing the operation of diodes and solar cells. It is worthwhile to mention that mobility and diffusion length are intimately connected to each other by the Einstein relation, $D = \mu k_B T$ where $D = L^2 t^{-1}$ is the diffusivity (and t is the carrier lifetime). Additionally, diffusion and drift, most of the time, occur concurrently, as has been shown in the past, for example, by Sze and Ghione.[50,51]

Finally, we consider the carrier lifetime *t*. This figure describes the time that the charges take to recombine under nonthermodynamic equilibrium situations, such as under photoexcitation. Carrier lifetime is related to the diffusion length and to the number of traps within the semiconductor (traps reduce t).

3.2. Techniques

The electrical mobility can be measured using a variety of techniques, as listed in **Table 2**. The Hall effect

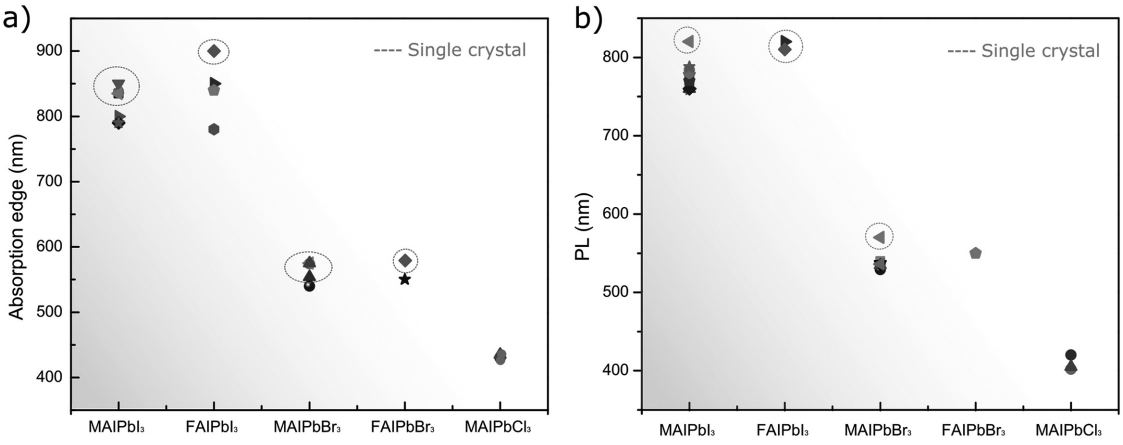

Figure 1. Spectral position of the a) absorption edge and b) PL peak for different lead halide perovskite compositions. The bandgap energy increases, progressing from iodine to chlorine. The spread in reported values may be attributable to variations in morphology and crystallinity, with more crystalline materials showing a red shift.

measurement[52] is one of the most widely used techniques. This technique allows one to not only measure the mobility but also to recognize the species of the major carriers responsible for conduction (electrons or holes). It is important to highlight a couple of experimental aspects. First, the Hall effect measurement is feasible only on sufficiently conductive samples. This requirement is often not met in perovskite thin films; these samples, have small thicknesses (on the order of 100 nm) and low mobilities (≤ 1 cm^2 V^{-1} s^{-1}), which leads to low conductivity. Second, Hall effect measurements can be affected by the properties of the electrical contacts (should be Ohmic) and by the quality of the material surface.[53] Third, in order to extract the mobility it is necessary to measure the resistivity of the material precisely (the four points technique or van der Pauw method are often used to achieve high precision).[54] In particular the van der Pauw method would require the patterning of the film in a characteristic "cloverleaf" shape; achieving such a pattern, that would ensure high precision in measuring the conductivity, is challenging for spin-coated perovskite films. Hall measurements probe the lateral mobility, specifically, the mobility of the carriers moving close to the surface. This quantity is particularly relevant for lateral devices such as FETs.

Another approach that has been used to measure mobility in perovskites is the space charge limited current (SCLC) method.[55–59] The transport within the semiconductor must be unipolar (electrons- or holes-only) and at least one of the two contacts must be Ohmic. This technique can be used to extract additional information (e.g., trap density) if performed as a function of temperature or light excitation.[60,61] The electrical contacts play a key role in the accuracy of the measurement. Series resistance or small energetic barriers give rise to side effects in the measurement and complicate the analysis of the results, leading in some cases to over- (or under-) estimation of the mobility.[62] This technique has been widely used in the past for characterizing organic materials. SCLC curves depend on many parameters such as temperature, nature of the contacts (interface barriers, series resistance can importantly affect the shape of the IV curves), kind of transport (diffusion currents are not always negligible, depending on the material and the structure of the device under test) and therefore require particular attention when designing the experiments.

A robust method to measure m is the time of flight (ToF) technique.[63–65] This method can be used to measure the mobility of both electrons and holes by changing the polarity of the applied bias. ToF requires an Ohmic and a noninjecting contact. The Ohmic contact needs to be transparent for photoexcitation. A limitation of this method resides in the requirement of an adequate sample thickness to obtain a measurable transit time. It is also noteworthy that the voltage should be high enough to ensure a significant photocurrent signal. The ToF measurement presents several advantages. First, it is a direct approach since mobility can be extracted directly from the transit time. Second, unlike the surface-probing Hall effect method, ToF is a bulk measurement and probes the vertical mobility, that is the mobility of carriers moving normal to the surface. This measurement is therefore particularly relevant for vertical devices such as LEDs and solar cells.

Another quality describing the electrical transport in semiconductors is the diffusion length. A long diffusion length is particularly important for photovoltaic materials since it is one of the crucial parameters for efficient photocarrier collection. Diffusion lengths can be measured in many ways. A common one involves the fabrication of rectifying diodes where the dominant conduction mechanism is diffusion. Measurements of the PL intensity of the diodes with different active layer thicknesses can be used to extract the diffusion length.[66,67]

A widely used method for perovskite thin films leverages the PL quenching ability of hole- or electron-transporting materials deposited on the perovskite films.[19,68,69] The optical methods have the advantage of avoiding mechanical perturbation in the materials, in contrast to the electrical methods where the deposition of the contacts, as well as the application of strong biases or the injection of large currents may damage the materials under test.

Finally, we consider the carrier lifetime. This quantity can be estimated by fitting the decay of the photoluminescence using a single or multiple exponential model.[70,71] Due to its simplicity, this method is also often used to assess the quality of materials; it should be noted though that carrier lifetime has no

Table 2. Electrical properties.

Property	Mobility	Lifetime	Diffusion length
Techniques	Hall effect: the mobility can be extracted from the voltage (the so called Hall voltage) generated in the direction perpendicular to the charge transport under a constant magnetic field.	PL lifetime: the decay time constant is extracted through fitting the PL decay.	Rectifying diodes: the PL of diodes of different thicknesses is used.
	SCLC: by analyzing the super-Ohmic regions in the current–voltage (*I–V*) curve of low conductivity semiconductors.		PL quenching method: the PL decay in the active materials in the presence of a PL quenching layer is analyzed using a transport model to extract the diffusion length.
	ToF: the transit time of photocarriers (excited by a flash lamp) as a function of the bias is used to extract the mobility. TRMC: mobility is extracted by analyzing the perturbation of the microwave absorbance.		Indirect calculation: the diffusion length is calculated from mobility and lifetime using the Einstein relation.

direct bearing on electrical transport, and therefore the mobility and diffusion length remain fundamental quantities to extract in order to characterize optoelectronic materials. Carrier lifetime can be used in combination with the mobility to estimate the diffusion length; this approach is particularly useful when a direct measurement of the diffusion length is difficult (for example in single crystals).[16]

3.3. Materials

Lead halide perovskites exhibit impressive electronic properties considering their solution-processed fabrication; nevertheless, these properties are continuously improved as the fabrication techniques of the materials are advanced. In **Figure 2**a, we plot the improvement of the diffusion length through recent years of research. Remarkably, the diffusion length increased from values well below 1 µm to exceeding 10 µm in about 3 years.[19,26,72–76] This improvement reflects the progress that has been recently made in producing solids with better structural order and morphology. As can be seen in Figure 2b, the diffusion length has a strong dependence on the grain size of the film. Diffusion lengths well above 1 µm have been achieved by realizing films with an average grain size exceeding 2 µm. The highest measured diffusion lengths are found in perovskite single crystals where values above 10 µm are found[6,16,17,77].

The simplest protocol for fabricating perovskite thin films is through direct spin coating of a single precursor solution containing both the lead source and organic source (such as CH_3NH_3I with PbI_2 for fabricating $CH_3NH_3PbI_3$), known as the one-step method.[78] Despite its simplicity, this procedure, applied in the early history of fabricating hybrid perovskite-based devices, usually produces perovskite films with branched structures, ≈100 nm grain sizes, and inhomogeneous morphologies, resulting in poor device performance.[79] Stranks et al. found that using a Cl-containing precursor recipe: $PbCl_2$ and CH_3NH_3I with a molar ratio of 1:3, instead of equimolar CH_3NH_3I and PbI_2, could produce better-coverage perovskite films with much improved electron and hole diffusion lengths (over 1 µm compared to ≈100 nm, measured by the selective PL quenching method).[19,75] It was found that excess CH_3NH_3Cl would be released during the annealing process, resulting in the formation of so-called $CH_3NH_3PbI_{3-x}Cl_x$ (although later it was found that the amount of Cl^- in the final perovskite was negligible).[18] Some researchers have proposed that the slight amount of chloride ion doping in $CH_3NH_3PbI_3$ could have resulted in the striking increase of carrier diffusion lengths,[80,81] in spite of the fact that the amount of Cl^- was

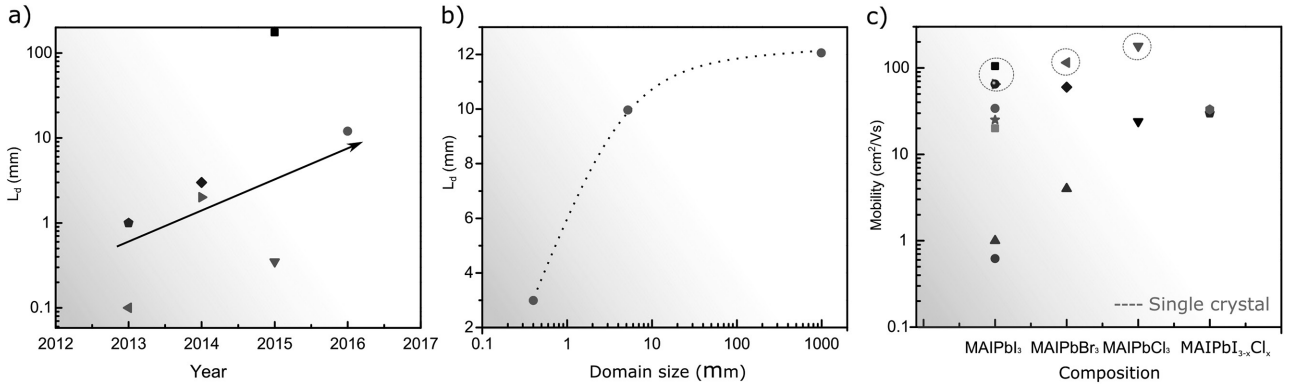

Figure 2. a) Measured diffusion length in lead halide perovskites as a function of the year reported. Increases are attributed to advances in materials processing and fabrication. b) Diffusion length as a function of the average grain (domain) size. c) Mobility for different perovskite compositions following the iodine to chlorine progression, and the special mixed iodine–chlorine case.

hardly detectable. Other researchers tended to attribute the enhanced carrier transport to the improved film morphology and crystallinity. Williams and co-workers carried out a thorough study on the crystallographic textures and grain structures of both films, and revealed that the $CH_3NH_3PbI_{3-x}Cl_x$ film was comprised of interconnected grains with preferred crystallographic orientations and much longer lattice coherence order than the $CH_3NH_3PbI_3$ film, which could be the reason for its superior optoelectronic properties. The role of chloride was assumed to be in the formation of certain intermediate phases with CH_3NH_3I and PbI_2, thus retarding the perovskite formation reaction and resulting in uniform nucleation for crystallization. This film formation theory is in line with other reports that used excess MACl as additives in the $CH_3NH_3PbI_3$ precursor solution to obtain smooth, continuous films and demonstrate similar high-efficiency perovskite solar cells.[1] Further evidence of the positive correlation of carrier diffusion lengths and grain sizes were provided by Hutter and co-workers in a comprehensive study of the electronic properties in planar and mesostructured $CH_3NH_3PbI_3$ and $CH_3NH_3PbI_{3-x}Cl_x$ films by time-resolved microwave conductivity (TRMC) and PL measurements.[73] They revealed diffusion lengths of over 10 and 4.1 μm in $CH_3NH_3PbI_{3-x}Cl_x$ (grain sizes >5 μm) and $CH_3NH_3PbI_3$ films (grain sizes ≈0.5 μm), respectively. The diffusion lengths decreased to ≈1.5 μm when the grain sizes of both films were restricted to 0.05 μm through the confined perovskite formation in a mesostructured Al_2O_3 layer.

In contrast to the one-step method, a two-step method where the deposition of lead salts and organic salts is decoupled into consecutive procedures has been demonstrated to be more flexible and efficient for fabricating high-quality perovskite films. In the early days of perovskite solar cell research, the two-step method consisted of a first step of depositing lead halide films and a following step of converting the lead halide films into perovskites by dipping them in an organic source solution.[82] This method produces thin films of discrete perovskite particles with sizes ranging from tens to hundreds of nanometers, and was demonstrated for fabricating reproducible, high-efficiency perovskite solar cells. A study on the carrier mobilities of the $CH_3NH_3PbI_3$ films prepared with both the one- and two-step methods showed values of 17 and 20 $cm^2\ V^{-1}\ s^{-1}$ (measured by TRMC at 9 GHz), respectively, which were correlated positively with the grain sizes.[83] However, the second step by dipping is problematic for fabricating planar perovskite solar cells due to the rough surface morphology of as-fabricated films and the incomplete conversion of lead halide to perovskites, even in a prolonged dipping process.[84]

Several strategies have been developed to improve this method. For example, Wu and co-workers found that spin coating the solution of PbI_2 in dimethyl sulfoxide (DMSO) instead of the commonly used solvent dimethyl formamide (DMF) would yield amorphous PbI_2 films in the form of DMSO/PbI_2 complexes. The retarded crystallization of PbI_2 would benefit from the intercalation of the organic source with PbI_2 to produce homogeneous perovskite films composed of large, uniform grains, and thus resulting in better-performance perovskite solar cells with higher reproducibility. In addition, other methods to convert the lead halide to perovskites, aside from dipping, were proposed, including spin coating of an organic source solution, i.e., the bilayer interdiffusion method,[85] and thermal evaporation of an organic powder source, i.e., the vapor-assisted solution process.[86] These methods provide better control over the reaction of organic source and lead halide through a slow perovskite formation process, and therefore can produce pin-hole-free, uniform films. Furthermore, Dong and co-workers revealed that, through multiple cycles of spin-coating MAI/MACl mixture solution on top of the PbI_2 film, abnormal crystal growth could be realized and micrometer-scale grains could be obtained. They further found that, with the increase of the perovskite grain size, the charge extraction time of the real device was significantly reduced, indicating improved charge carrier mobilities of the perovskite films.[85]

The carrier mobility has also been improved over the years and exhibits dependence on the morphology. Mobilities exceeding 10 $cm^2\ V^{-1}\ s^{-1}$ have been measured in perovskite films[27,73,74,83,87] (particularly Cl–I mixtures as previously mentioned) and above 100 $cm^2\ V^{-1}\ s^{-1}$ (using ToF measurements) in perovskite single crystals. As can be seen in Figure 2c, the mobility (as also the diffusion length) does not exhibit a strong dependence on the material composition. The mobility of thin films has been also measured using FETs and assessed to be ≈1 $cm^2\ V^{-1}\ s^{-1}$.[87,88] It is important to note that FET mobility can be easily over- or underestimated as a result of effects related to the semiconductor/oxide interface.

Finally, we direct attention to carrier lifetime. As previously mentioned this quantity is widely used to characterize perovskite solids; although carrier lifetime gives a measure of the quality of the film (we recall t directly has a dependence on the defects) we stress that a proper characterization of a material involves the extraction of mobility and/or diffusion length.[89] Carrier lifetimes in excess of 1 μs have been measured from PL decay.[19] Much longer decays have been shown using different techniques involving electrical measurements (e.g., photovoltage decay).[17] In such measurements, it is important to discern the decay that originates from recombination from the decay that is due to capacitive effects, which are usually convoluted with one another.

In brief, the advancement of perovskite-based devices, especially solar cells, has been closely correlated with the development of the deposition techniques used to obtain high-quality (with regard to both crystallinity and morphology) perovskite thin films, since the intrinsic electronic properties of hybrid perovskites in the thin films mainly depends on these factors. The crystallinity of a film directly determines the defect densities and their distributions, which are crucial parameters influencing the electronic properties. To be more specific, the density of grain boundaries (and so grain sizes), one important aspect used to evaluate the crystallinity and morphology of a thin film, will strongly influence the charge transport in the films because the transport among crystalline grains is, in general cases, strongly deteriorated by the charge localization, scattering and intensive trapping at the boundaries. These will be discussed in detail in the next section.

4. Trap States

Trap states, especially those located deeply in the forbidden bandgap, are detrimental to charge transport. Deep trap states can act as nonradiative recombination centers, thereby reducing charge carrier lifetimes; whereas shallow trap states may act as scattering centers, which also have negative impacts on charge transport. Defect-assisted recombination is a mechanism competing with radiative recombination and is thus detrimental for light-emitting devices. Additionally, defect-assisted recombination reduces the open-circuit voltage in photovoltaic devices. Therefore, materials with a low trap density are highly desirable. At the same time, a thorough investigation of the properties of the traps is crucial for designing efficient devices.

Extensive theoretical and experimental investigations of traps in perovskite solids have been carried out. Values of 10^{14}–10^{17} cm^{-3} for the densities of the deep as well as the shallow trap states in perovskite thin films have been measured by several groups using different methods.[9,73,90,91] In contrast, calculations from defect energetics have predicted that the intrinsic defect states in perovskites are prone to lie close to the valence or conduction band.[92,93] This discrepancy requires further improvement of the simulation models, as well as experimental work to clarify the origin and distribution of defects. Furthermore, it remains a puzzle how a small voltage loss can be achieved in perovskite solar cells with these nonnegligible subgap defect states. A recently proposed slow trap-mediated recombination mechanism may be able to explain the high V_{OC} (≈1.2 V) that is achieved in state-of-art perovskite solar cells.[94]

Another debate focuses on the defect states at the grain boundaries in perovskite thin films. In general cases, defect states will accumulate at the surface of crystalline grains due to enriched dangling bonds and unsatisfied stoichiometry. Interestingly, calculations predicted the benignity of the grain boundaries by revealing the shallow energetic levels of the defect states,[37] which were also confirmed experimentally by some groups.[95,96] Yet, this viewpoint was challenged recently by the observation of relatively weaker local PL emission from the grain boundaries than from the grain interior, indicating stronger nonradiative recombination at the boundaries. Furthermore, the areas with weak PL can be improved through passivation.[89] Therefore, it seems that the trap states in the hybrid perovskite films are not negligible as previously expected, and that passivation which targets nonradiative recombination paths is an effective route toward pushing the performance of perovskite solar cells toward their Shockley–Queisser limit. Various materials have been found to be capable of achieving this goal, such as fullerene derivatives, Lewis acids, and Lewis bases.[97–99] In addition, it is not difficult to imagine that increasing the grain sizes so as to reduce the density of grain boundaries would also be an efficient way to reduce the overall defect densities in the thin films, and further improve the charge carrier lifetime, mobility, diffusion length, and, ultimately, device performance. This notion has been supported by several experimental works.[100,101]

The interfaces formed between perovskites and the other layers of a device are another crucial factor. Specifically, this is important when considering defects, since the defects at the interfaces may not only form intrinsically during the growth of perovskite thin films (i.e., defects at the grain boundaries), but also may be generated or suppressed from the interaction with other device components. For example, Huang and coworkers found that perovskite thin films deposited on c-OTPD (crosslinked *N*4,*N*4′-bis(4-(6-((3-ethyloxetan-3-yl)methoxy) hexyl)phenyl)-*N*4,*N*4′-diphenylbiphenyl-4,4′-diamine) had less bottom surface traps compared to those on poly(3,4-ethylenedioxythiophene) polystyrene sulfonate.[102] 4-tert-butylpyridine, a commonly used dopant in the hole-transporting materials of perovskite solar cells, was reported to be corrosive for perovskites and thus produces additional defects.[103] In addition, the interfacial traps in perovskite solar cells are especially interesting for their suspected roles in the well-known hysteresis problem of *I*–*V* measurements.[99,104] Extensive works have looked at choosing appropriate interface layers to improve the efficiency of charge extraction from the perovskites.[105] It is worth noting that this improvement of charge extraction through interface layers has been sometimes explained by side effects such as the higher mobilities and energy level tailoring of the interface layers.[106,107] Despite this, their potential passivation effects should also be considered.

The recent successful synthesis of perovskite single crystals in millimeter dimensions enabled the characterization of trap densities and the in gap distribution in these materials in their purest form. The previously discussed SCLC method can be also used to measure these quantities.[57,62] For sufficiently high current densities, the relation between current and voltage deviates from Ohm's law. The semiconductor is, in fact, unable to relocate enough charge and a spatial charge forms within the solid. Such a spatial displacement of charge is responsible for a deformation of the electric field within the semiconductor and ultimately for a nonlinear *I*–*V* relation (super-Ohmic behavior). If a distribution of traps is present at a characteristic energy close to the Fermi energy (deep traps), these traps will be filled when the Fermi level moves as a result of the accumulation of spatial charge in the solid. The sudden filling of deep traps causes a steep increase in the *I*–*V* curve following a law: $I = V^n$ with $n \geq 3$. The onset voltage can be then used to extract the trap density.

Temperature is another variable that can be used to modulate the Fermi–Dirac distribution (i.e., the density of free carriers within the solid) within the bandgap. It is therefore also possible to extract the density of trap states through temperature-dependent *I*–*V* curves.

SCLC has been performed on perovskite single crystals independently by several groups. The results are highly consistent. Total trap densities as low as ≈10^9 cm^{-3} for states close to the valence band have been reported. A refined temperature-dependent version of this characterization was performed by Adinolfi *et al.*[108] on $MAPbI_3$ single crystals. They reported that a distribution of traps (10^9–10^{10} cm^{-3}) was present at ≈0.1 eV above the valence band and a distribution of traps, slightly more populated (≈10^{11} cm^{-3}), was found at ≈0.15 eV below the conduction band. These results align well with theoretical predictions made using DFT simulations.

Despite the ambiguity of the density and distribution of trap states in perovskite thin films, it seems clear that perovskite single crystals have profoundly lower trap densities compared to the thin films, and therefore are potentially more advantageous

for applications. A perovskite film composed of large grains is a route to approaching the single crystal limit and also easier to be realized. As the bulk properties of perovskite thin films are being continuously improved with the advancement of film deposition techniques, the interfaces are becoming of increasing importance.

5. Devices

The ultimate goal of materials research is to realize efficient devices that address the needs of the market and improve the quality of our lives. The balance achieved between facile fabrication and strong electronic properties makes perovskites excellent candidates as photovoltaic and light -mitting materials. The importance of these applications in the energy and environmental context has made perovskites one of the focal points of materials science in the last few years. In this section, we correlate the fundamental properties of materials with their impacts on device performance.

Solar cells are by far the most studied devices within the context of perovskites.[27,76,109] Perovskites are good photovoltaic materials for several reasons. First, since they are direct bandgap materials, they are able to absorb almost the entirety of the visible to near-infrared solar radiation over a thickness below 1 μm. Second, the bandgap of $MAPbI_3$ (or FAI/MAI) is close to the 1.3 eV optimal value estimated by Queisser and Shockley. Third, perovskite films exhibit a low concentration of traps, enabling high photovoltage (V_{OC}) and long diffusion lengths (>1 μm), which are necessary for efficient collection of photocharges. Last but not least, these materials are ambipolar[88] (i.e., the transport properties of electron and holes are comparable) and mildly doped, allowing the fabrication of p–i–n like structures employing an extracting built-in electric field that enhances charge collection. Thanks to these material properties, the power conversion efficiency (PCE) of perovskite solar cells (laboratory prototypes for now) is already competitive with commercial technologies such as silicon, cadmium telluride, and CIGS (cadmium indium gallium selenide) solar cells.[2,110] Given that recent improvements of perovskite film qualities have increased the diffusion length largely beyond the thickness necessary to completely absorb the incident light, it would be reasonable to assume that additional improvements in the film qualities would not contribute big increments to the PCE. In **Figure 3**a, we show simulations of PCE as a function of the perovskite layer's diffusion length, illustrating a plateau-like behavior. However, a recent demonstration of the first prototype perovskite monocrystalline solar cells raised the prospect of perovskite single crystals achieving comparable performance to state-of-the-art perovskite thin film solar cells, yet providing a comparably simpler device architecture.[38] This study suggests the pursuit of even higher-crystallinity perovskite films is still intriguing.

Despite the outstanding progress of perovskite solar cells, several issues need to be addressed before their commercialization. The most pertinent of all is the material stability. Photovoltaic material is required to be stable at relatively high temperatures (≈80 °C), to atmospheric agents, and to moisture for several years. So far perovskite materials have proven to be quite unstable and the origin of this instability is not well understood; at the same time, a precise strategy to address this problem is missing.[111,112] Another element to keep in mind to further improve the performance of these devices is the optimization of the contacts, optically and electrically. The quality of the contacts in terms of transparency, electrical properties, and quality of the interface are crucial. An excellent example of how important these components of a solar device is represented by heterojunction solar cells, where dramatic advances have been achieved in the last few years, working exclusively on the contact area.[113,114] At the same time, this consideration should discourage the practice of assessing the properties of the materials from the performance of the device, because the device's performance is affected by several factors, many independent from the active material. Deconvoluting the innate material information from the device performance is, in practice, not feasible.

Light detection and emission applications are also rapidly expanding fields thanks to advances in perovskite materials. These applications can benefit greatly from the materials' ease

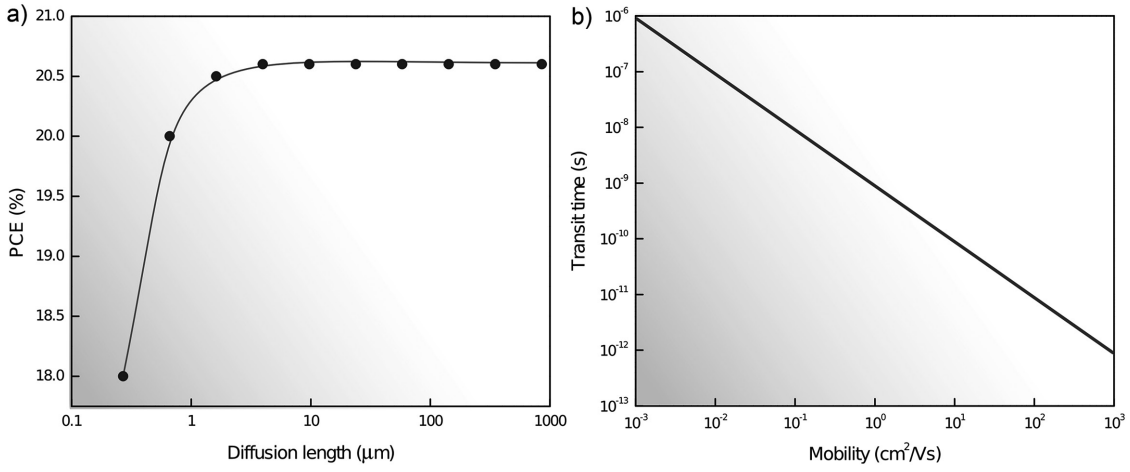

Figure 3. a) Simulation of the PCE for a perovskite solar cell as a function of the diffusion length. The PCE saturates for a value of L_{diff} close to the active-layer thickness (400 nm in the model). b) Transit time in a 200-nm-thick photodiode as a function of the semiconductor mobility.

of tunability, which enables adjustable emission and absorption within the visible to near-IR spectrum of light. Efficient perovskite photodetectors were realized in the last few years. A multitude of architectures were proposed,[3,4,115–119] particularly for photodiodes. It was noted that the choice of the contacts plays a major role, largely influencing the responsivity of the devices. Interface traps can add photoconductive gain to perovskite photodiodes, resulting in increased recombination and higher dark current. Perovskite-based visible light detectors achieve high detectivity, reaching 10^{13} Jones and quantum efficiencies above unity. It has been recently demonstrated that the performance of photodetectors can be further improved by using high-crystallinity materials. A $MAPbBr_3$ single crystal-integrated photodetector has been presented showing the highest gain and gain-bandwidth product.[6] This performance is the result of the superior material properties of perovskite single crystals and a control over the material morphology that afforded the fabrication of small devices with a characteristic channel length of 5 µm. Single crystals have also been used to fabricate interesting architectures producing a narrowband response.[38] These detectors leverage the high surface recombination of perovskite single crystals to cut the response of the device at frequencies above the bandgap. Although the mobility of perovskites can be as high as >100 $cm^2\ V^{-1}\ s^{-1}$, the speed of photodetectors is still limited to ≈1.6 MHz due to the relatively thick active layer (≈>0.9 mm). This limitation was overcome by Saidaminov *et al.*, employing a planar integrated single crystalline film with contact spacings of 5 µm, thus realizing tunable narrow band photodetectors with bandwidths of around 33 kHz.[120] Even if a photodiode can, in principle, be limited in its speed by the transit time, perovskite detectors still suffer from traps at the contact interface and hysteretic effects inherent to the materials. In Figure 3b we plot, for reference, the theoretical speed (transit time for a thickness of 200 nm) achievable as a function of the mobility.

The response of photodetectors is quantified using figures of merit such as the quantum efficiency (external EQE, and internal IQE) defined as the number of generated carriers per incident (or absorbed) photon, and responsivity defined as photo—current/incident optical power. These figures of merit are largely affected by the mobility of the material (especially in photoconductors and photoconductive diodes) and the recombination properties of the films (traps). While mobility plays a major role in a photoconductive architecture, in photodiodes (unity gain) the key parameter is the diffusion length, as previously discussed for solar cells. Mobility also affects the response time of the detectors. In order to achieve fast response time, it is desirable to cut off photoconductive gain (usually assisted by long-lifetime trap states) and therefore use rectifying structures (metal–semiconductor–metal devices, diodes). As per the detectivity (defined as $D^* = R \times A^{1/2}/{i_n}^{1/2}$), it is important to achieve high QE (or responsivity, equivalently) and very low dark current (which increases substantially the noise current, i_n). High D^* values can be achieved by suppressing the dark current using low-trap materials, which produce small recombination currents. Interfaces also play an important role and must be engineered in such a way to decrease interface recombination and leakage currents.

LEDs offer a distinct set of considerations from detectors and solar cells.[121,122] The dominant factor governing these devices is the ratio between radiative and nonradiative recombination. Nonradiative recombination due to traps (e.g., Shockley–Reed–Hall recombination) or the Auger effect can be reduced by reducing the amount of traps within the solid. With this regard, effort can be spent on improving the material morphology and stoichiometry, which have the greatest effect on defect state density. Alternatively, the radiative recombination efficiency depends on many factors inherent in the material such as the exciton binding energy and the electric permittivity. The device architecture can greatly enhance the performance of LEDs. Confined structures such as quantum wells and quantum dots favor radiative recombination by strengthening the binding energy of the excitons. Perovskite colloidal quantum dots are in the early stages of development. These materials are extremely flexible in terms of bandgap tunability since this can be achieved simultaneously by using the quantum size effect and the stoichiometry of the perovskite material.

One of the key areas of investigation for perovskite-based devices is determining the branching fraction between excitons and free carriers, and the exciton binding energy. This is an active topic of research. Many recent articles have shown that the exciton binding energy for $MAPbI_3$ is extremely low, at only a few millielectron volts,[44,123,124] such that phonon interactions lead to nearly full ionization of excitons,[125] and that free carrier generation occurs upon light absorption.[123,124] These observations have been made using a variety of techniques including transient absorption spectroscopy,[126] electroabsorption spectroscopy,[124] and temperature-dependent spectroscopy.[125] The long diffusion length of hybrid perovskites further suggests that this is the case. The primarily nonexciton character of $MAPbI_3$ is advantageous for solar cells since carriers freely dissociate, as in the case of inorganic solar cells, instead of requiring a heterostructure interface to induce dissociation, as in the case of organic solar cells. The exciton binding energy has been shown to increase following the iodine to bromine to chlorine progression.[34,127] The morphology of the perovskite has also been shown to impact the exciton binding energy. It was seen that smaller crystals or more polycrystalline films exhibit suppressed exciton formation due to lattice variations that cause variations in electrostatic potential which screen the electron–hole interactions.[126] Nanocrystals, particularly ultrathin nanoplatelets of $MAPbBr_3$, have shown much higher binding energies due to reduced screening as a result of delocalization of the electric field between electron and hole to regions outside the high-dielectric constant perovskite.[128] Research on the exciton binding energy is not only central to solar cells, but also to light emission devices, as the exciton binding energy greatly impacts the excited state population and is a factor in the dominating recombination pathways.[127,129]

6. Conclusions

We presented an overview of the fundamental optical, transport, and photophysical properties that govern the performance of perovskite-based optoelectronic devices. These parameters can be summarized in key attributes: bandgap, mobility,

diffusion length, charge-carrier lifetime, and defect-trap density. In the past few years, perovskite materials have made great strides in improving these attributes as a result of improving material morphology, which has made perovskites—despite their low-temperature solution processibilty—into a compelling and established field of semiconductors. There still remains a significant spread in the reported values of the material properties, highlighting not only the sensitivity of perovskite properties to the material's morphologies and processing conditions (especially precursor stoichiometry) but also the multitude of approaches utilized to extract these properties. We described the most robust methodologies for investigating the key attributes, and the subtle differences between them and precautions that should be taken in interpreting the data obtained from each approach, which we believe will lead to more uniform reported values in the future.

Broadly speaking, each of the mentioned attributes is significant for all optoelectronic applications, but with varying importance. For the three most widely investigated optoelectronic applications of perovskites—solar cells, photodetectors, and LEDs—we described which figures are paramount, and which are ancillary. The comprehensive analysis encompassed in this review provides a vantage point from which we can present guidelines to direct the efforts of the research community.

For solar cells, both mobility and diffusion length are crucial, yet those two attributes have already reached reasonable values in state-of-the-art thin films, to the point where it seems that interfacial engineering and stability are currently more pertinent issues that require addressing. Photodectors, on the other hand, still stand to benefit from improving the transit time, which still scales well with improvements in mobility and device architecture. Finally, LEDs are acutely sensitive to the radiative lifetime and the suppression of nonradiative pathways, which implies that quantum-confined perovskites, such as nanocrystals and so-called low-dimensional perovskite derivatives, offer a more fruitful path for achieving efficient devices than canonical hybrid perovskites.

Keywords

composition, hybrid, mobility, traps, perovskites

Received: February 7, 2017
Published online:

[1] M. M. Lee, J. Teuscher, T. Miyasaka, T. N. Murakami, H. J. Snaith, *Science* **2012**, *338*, 643.
[2] W. S. Yang, J. H. Noh, N. J. Jeon, Y. C. Kim, S. Ryu, J. Seo, S. I. Seok, *Science* **2015**, *348*, 1234.
[3] R. Dong, Y. Fang, J. Chae, J. Dai, Z. Xiao, Q. Dong, Y. Yuan, A. Centrone, X. C. Zeng, J. Huang, *Adv. Mater.* **2015**, *27*, 1912.
[4] L. Dou, Y. M. Yang, J. You, Z. Hong, W.-H. Chang, G. Li, Y. Yang, *Nat. Commun.* **2014**, *5*, 5404.
[5] E. Edri, S. Kirmayer, D. Cahen, G. Hodes, *J. Phys. Chem. Lett.* **2013**, *4*, 897.
[6] M. I. Saidaminov, V. Adinolfi, R. Comin, A. L. Abdelhady, W. Peng, I. Dursun, M. Yuan, S. Hoogland, E. H. Sargent, O. M. Bakr, *Nat. Commun.* **2015**, *6*, 8724.
[7] H.-R. Xia, J. Li, W.-T. Sun, L.-M. Peng, *Chem. Commun.* **2014**, *50*, 13695.
[8] B. R. Sutherland, S. Hoogland, M. M. Adachi, C. T. O. Wong, E. H. Sargent, *ACS Nano* **2014**, *8*, 10947.
[9] G. Xing, N. Mathews, S. S. Lim, N. Yantara, X. Liu, D. Sabba, M. Grätzel, S. Mhaisalkar, T. C. Sum, *Nat. Mater.* **2014**, *13*, 476.
[10] H. Zhu, Y. Fu, F. Meng, X. Wu, Z. Gong, Q. Ding, M. V. Gustafsson, M. T. Trinh, S. Jin, X.-Y. Zhu, *Nat. Mater.* **2015**, *14*, 636.
[11] W. Peng, J. Yin, K.-T. Ho, O. Ouellette, M. D. Bastiani, B. Murali, O. E. Tall, C. Shen, X. Miao, J. Pan, E. Alarousu, J.-H. He, B. S. Ooi, O. F. Mohammed, E. Sargent, O. Bakr, *Nano Lett.* **2017**, *17*, 4759.
[12] M. I. Saidaminov, A. L. Abdelhady, G. Maculan, O. Bakr, *Chem. Commun.* **2015**, *51*, 17658.
[13] Y. Liu, Z. Yang, D. Cui, X. Ren, J. Sun, X. Liu, J. Zhang, Q. Wei, H. Fan, F. Yu, X. Zhang, C. Zhao, S. F. Liu, *Adv. Mater.* **2015**, *27*, 5176.
[14] J. M. Kadro, K. Nonomura, D. Gachet, M. Grätzel, A. Hagfeldt, *Sci. Rep.* **2015**, *5*, 11654.
[15] T. Zhang, M. Yang, E. E. Benson, Z. Li, J. van de Lagemaat, J. M. Luther, Y. Yan, K. Zhu, Y. Zhao, *Chem. Commun.* **2015**, *51*, 7820.
[16] D. Shi, V. Adinolfi, R. Comin, M. Yuan, E. Alarousu, A. Buin, Y. Chen, S. Hoogland, A. Rothenberger, K. Katsiev, Y. Losovyj, X. Zhang, P. A. Dowben, O. F. Mohammed, E. H. Sargent, O. M. Bakr, *Science* **2015**, *347*, 519.
[17] Q. Dong, Y. Fang, Y. Shao, P. Mulligan, J. Qiu, L. Cao, J. Huang, *Science* **2015**, *347*, 967.
[18] H. Yu, F. Wang, F. Xie, W. Li, J. Chen, N. Zhao, *Adv. Funct. Mater.* **2014**, *24*, 7102.
[19] S. D. Stranks, G. E. Eperon, G. Grancini, C. Menelaou, M. J. P. Alcocer, T. Leijtens, L. M. Herz, A. Petrozza, H. J. Snaith, *Science* **2013**, *342*, 341.
[20] C. Roldán-Carmona, O. Malinkiewicz, A. Soriano, G. Mínguez Espallargas, A. Garcia, P. Reinecke, T. Kroyer, M. I. Dar, M. K. Nazeeruddin, H. J. Bolink, *Energy Environ. Sci.* **2014**, *7*, 994.
[21] D. L. Wood, J. Tauc, *Phys. Rev. B* **1972**, *5*, 3144.
[22] F. Yang, M. Wilkinson, E. Austin, K. O'Donnell, *Phys. Rev. Lett.* **1993**, *70*, 323.
[23] C. Delerue, G. Allan, C. Reynaud, O. Guillois, G. Ledoux, F. Huisken, *Phys. Rev. B* **2006**, *73*, 235318.
[24] J. Linnros, N. Lalic, A. Galeckas, V. Grivickas, *J. Appl. Phys.* **1999**, *86*, 6128.
[25] S. De Wolf, J. Holovsky, S.-J. Moon, P. Löper, B. Niesen, M. Ledinsky, F.-J. Haug, J.-H. Yum, C. Ballif, *J. Phys. Chem. Lett.* **2014**, *5*, 1035.
[26] J. H. Heo, D. H. Song, H. J. Han, S. Y. Kim, J. H. Kim, D. Kim, H. W. Shin, T. K. Ahn, C. Wolf, T. W. Lee, S. H. Im, *Adv. Mater.* **2015**, *27*, 3424.
[27] C. S. Ponseca, T. J. Savenije, M. Abdellah, K. Zheng, A. Yartsev, T. Pascher, T. Harlang, P. Chabera, T. Pullerits, A. Stepanov, J. P. Wolf, V. Sundström, *J. Am. Chem. Soc.* **2014**, *136*, 5189.
[28] C. Motta, F. El-Mellouhi, S. Sanvito, *Sci. Rep.* **2015**, *5*, 12746.
[29] C. Wehrenfennig, G. E. Eperon, M. B. Johnston, H. J. Snaith, L. M. Herz, *Adv. Mater.* **2014**, *26*, 1584.
[30] R. Hull, *Properties of Crystalline Silicon*, IET, London, UK **1999**.
[31] B. Wang, Y. K. Wong, S. Yang, T. Chen, *J. Mater. Chem. A* **2016**, *4*, 3806.
[32] R. Sheng, A. Ho-Baillie, S. Huang, S. Chen, X. Wen, X. Hao, M. A. Green, *J. Phys. Chem. C* **2015**, *119*, 3545.
[33] E. Edri, S. Kirmayer, D. Cahen, G. Hodes, *J. Phys. Chem. Lett.* **2013**, *4*, 897.
[34] R. Comin, G. Walters, E. S. Thibau, O. Voznyy, Z.-H. Lu, E. H. Sargent, *J. Mater. Chem. C* **2015**, *3*, 8839.
[35] K. T. Butler, J. M. Frost, A. Walsh, *Mater. Horiz.* **2015**, *2*, 228.

[36] P. Schulz, E. Edri, S. Kirmayer, G. Hodes, D. Cahen, A. Kahn, *Energy Environ. Sci.* **2014**, *7*, 1377.
[37] W. J. Yin, T. Shi, Y. Yan, *Adv. Mater.* **2014**, *26*, 4653.
[38] Y. Fang, Q. Dong, Y. Shao, Y. Yuan, J. Huang, *Nat. Photonics* **2015**, *9*, 679.
[39] Y. Liu, Z. Yang, D. Cui, X. Ren, J. Sun, X. Liu, J. Zhang, Q. Wei, H. Fan, F. Yu, X. Zhang, C. Zhao, S. F. Liu, *Adv. Mater.* **2015**, *27*, 5176.
[40] H. Zhou, Z. Nie, J. Yin, Y. Sun, H. Zhuo, D. Wang, D. Li, J. Dou, X. Zhang, T. Ma, *RSC Adv.* **2015**, *5*, 85344.
[41] P. Khoram, S. Brittman, W. I. Dzik, J. N. H. Reek, E. C. Garnett, *J. Phys. Chem. C* **2016**, *120*, 6475.
[42] W. Peng, L. Wang, B. Murali, K.-T. Ho, A. Bera, N. Cho, C.-F. Kang, V. M. Burlakov, J. Pan, L. Sinatra, C. Ma, W. Xu, D. Shi, E. Alarousu, A. Goriely, J.-H. He, O. F. Mohammed, T. Wu, O. M. Bakr, *Adv. Mater.* **2016**, *28*, 3383.
[43] G. Maculan, A. D. Sheikh, A. L. Abdelhady, M. I. Saidaminov, M. A. Haque, B. Murali, E. Alarousu, O. F. Mohammed, T. Wu, O. M. Bakr, *J. Phys. Chem. Lett.* **2015**, *6*, 3781.
[44] Q. Lin, A. Armin, R. C. R. Nagiri, P. L. Burn, P. Meredith, *Nat. Photonics* **2015**, *9*, 106.
[45] P. Löper, M. Stuckelberger, B. Niesen, J. Werner, M. Filipič, S.-J. Moon, J.-H. Yum, M. Topič, S. De Wolf, C. Ballif, *J. Phys. Chem. Lett.* **2015**, *6*, 66.
[46] M. Sharizal Alias, I. Dursun, M. I. Saidaminov, E. Marwane Diallo, P. Mishra, T. N. Khee, O. M. Bakr, B. S. Ooi, *Opt. Express*, **2016**, *24*, 16586.
[47] J. M. Ball, S. D. Stranks, M. T. Hörantner, S. Hüttner, W. Zhang, J. W. Crossland, I. Ramirez, M. Riede, M. B. Johnston, U. Steiner, J. Henry, E. J. W. Crossland, I. Ramirez, M. Riede, M. B. Johnston, R. H. Friend, H. J. Snaith, *Energy Environ. Sci.* **2015**, *8*, 602.
[48] X. Ziang, L. Shifeng, Q. Laixiang, P. Shuping, W. Wei, Y. Yu, Y. Li, C. Zhijian, W. Shufeng, D. Honglin, Y. Minghui, G. G. Qin, *Opt. Mater. Express* **2014**, *5*, 29.
[49] R. A. Soref, *Proc. IEEE* **1993**, *81*, 1687.
[50] S. M. Sze, *Physics of Semiconductor Devices*, 3rd ed., Wiley, Hoboken, NJ, **2007**.
[51] F. L. Traversa, F. Bertazzi, F. Bonani, S. Donati Guerrieri, G. Ghione, S. Perez, J. Mateos, T. Gonzalez, *IEEE Trans. Electron Devices* **2010**, *57*, 1539.
[52] J. C. Male, *Br. J. Appl. Phys.* **1967**, *18*, 1543.
[53] R. Chwang, B. J. Smith, C. R. Crowell, *Solid-State Electron.* **1974**, *17*, 1217.
[54] A. A. Ramadan, R. D. Gould, A. Ashour, *Thin Solid Films* **1994**, *239*, 272.
[55] M. A. Lampert, *Phys. Rev.* **1956**, *103*, 1648.
[56] S. Nespurek, E. A. Silinsh, *Phys. Status Solidi* **1976**, *34*, 747.
[57] M. A. Lampert, A. Rose, R. W. Smith, *J. Phys. Chem. Solids* **1959**, *8*, 464.
[58] J. Dacuña, A. Salleo, *Phys. Rev. B: Condens. Matter Mater. Phys.* **2011**, *84*, 195209.
[59] M. Arif, M. Yun, S. Gangopadhyay, K. Ghosh, L. Fadiga, F. Galbrecht, U. Scherf, S. Guha, *Phys. Rev. B* **2007**, *75*, 195202.
[60] C. Krellner, S. Haas, C. Goldmann, K. P. Pernstich, D. J. Gundlach, B. Batlogg, *Phys. Rev. B: Condens. Matter Mater. Phys.* **2007**, *75*, 245115.
[61] P. Mark, W. Helfrich, *J. Appl. Phys.* **1962**, *33*, 205.
[62] F. Schauer, R. Novotny, S. Nešpůrek, *J. Appl. Phys.* **1997**, *81*, 1244.
[63] H. Li, L. Duan, D. Zhang, G. Dong, J. Qiao, L. Wang, Y. Qiu, *J. Phys. Chem. C* **2014**, *118*, 6052.
[64] H. Fujikake, T. Murashige, M. Sugibayashi, K. Ohta, *Appl. Phys. Lett.* **2004**, *85*, 3474.
[65] J. Isberg, J. Hammersberg, E. Johansson, T. Wikström, D. J. Twitchen, A. J. Whitehead, S. E. Coe, G. A. Scarsbrook, *Science* **2002**, *297*, 1670.
[66] D. Zhitomirsky, O. Voznyy, S. Hoogland, E. H. Sargent, *ACS Nano* **2013**, *7*, 5282.
[67] C. J. Hwang, *J. Appl. Phys.* **1969**, *40*, 3731.
[68] R. R. Lunt, N. C. Giebink, A. A. Belak, J. B. Benziger, S. R. Forrest, *J. Appl. Phys.* **2009**, *105*, 53711.
[69] G. E. Eperon, S. D. Stranks, C. Menelaou, M. B. Johnston, L. M. Herz, H. J. Snaith, *Energy Environ. Sci.* **2014**, *7*, 982.
[70] J. A. Giesecke, M. C. Schubert, B. Michl, F. Schindler, W. Warta, *Sol. Energy Mater. Sol. Cells* **2011**, *95*, 1011.
[71] R. K. Ahrenkiel, *Solid-State Electron.* **1992**, *35*, 239.
[72] K. Zheng, K. Zidek, M. Abdellah, M. E. Messing, M. J. Al-Marri, T. Pullerits, *J. Phys. Chem. C* **2016**, *120*, 3077.
[73] E. M. Hutter, G. E. Eperon, S. D. Stranks, T. J. Savenije, *J. Phys. Chem. Lett.* **2015**, *6*, 3082.
[74] C. Wehrenfennig, M. Liu, H. J. Snaith, M. B. Johnston, L. M. Herz, *Energy Environ. Sci.* **2014**, *7*, 2269.
[75] G. Xing, N. Mathews, S. Sun, S. S. Lim, Y. M. Lam, M. Grätzel, S. Mhaisalkar, T. C. Sum, *Science* **2013**, *342*, 344.
[76] Y. Zhao, A. M. Nardes, K. Zhu, *J. Phys. Chem. Lett.* **2014**, *5*, 490.
[77] A. A. Zhumekenov, M. I. Saidaminov, M. A. Haque, E. Alarousu, S. P. Sarmah, B. Murali, I. Dursun, X.-H. Miao, A. L. Abdelhady, T. Wu, O. F. Mohammed, O. M. Bakr, *ACS Energy* **2016**, *1*, 32.
[78] H.-S. Kim, C.-R. Lee, J.-H. Im, K.-B. Lee, T. Moehl, A. Marchioro, S.-J. Moon, R. Humphry-Baker, J.-H. Yum, J. E. Moser, M. Grätzel, N.-G. Park, *Sci. Rep.* **2012**, *2*, 591.
[79] M. Liu, M. B. Johnston, H. J. Snaith, *Nature* **2013**, *501*, 395.
[80] S. T. Williams, F. Zuo, C.-C. Chueh, C.-Y. Liao, P.-W. Liang, A. K.-Y. Jen, *ACS Nano* **2014**, *8*, 10640.
[81] S. Colella, E. Mosconi, P. Fedeli, A. Listorti, F. Gazza, F. Orlandi, P. Ferro, T. Besagni, A. Rizzo, G. Calestani, G. Gigli, F. De Angelis, R. Mosca, *Chem. Mater.* **2013**, *25*, 4613.
[82] J. Burschka, N. Pellet, S.-J. Moon, R. Humphry-Baker, P. Gao, M. K. Nazeeruddin, M. Grätzel, *Nature* **2013**, *499*, 316.
[83] H. Oga, A. Saeki, Y. Ogomi, S. Hayase, S. Seki, *J. Am. Chem. Soc.* **2014**, *136*, 13818.
[84] Y. Wu, A. Islam, X. Yang, C. Qin, J. Liu, K. Zhang, W. Peng, L. Han, *Energy Environ. Sci.* **2014**, *7*, 2934.
[85] Z. Xiao, C. Bi, Y. Shao, Q. Dong, Q. Wang, Y. Yuan, C. Wang, Y. Gao, J. Huang, *Energy Environ. Sci.* **2014**, *7*, 2619.
[86] Q. Chen, H. Zhou, Z. Hong, S. Luo, H.-S. Duan, H.-H. Wang, Y. Liu, G. Li, Y. Yang, *J. Am. Chem. Soc.* **2014**, *136*, 622.
[87] G. Wang, D. Li, H.-C. Cheng, Y. Li, C.-Y. Chen, A. Yin, Z. Zhao, Z. Lin, H. Wu, Q. He, M. Ding, Y. Liu, Y. Huang, X. Duan, *Sci. Adv.* **2015**, *1*, e1500613.
[88] X. Y. Chin, D. Cortecchia, J. Yin, A. Bruno, C. Soci, *Nat. Commun.* **2015**, *6*, 7383.
[89] D. W. deQuilettes, S. M. Vorpahl, S. D. Stranks, H. Nagaoka, G. E. Eperon, M. E. Ziffer, H. J. Snaith, D. S. Ginger, *Science* **2015**, *348*, 683.
[90] H.-S. Duan, H. Zhou, Q. Chen, P. Sun, S. Luo, T.-B. Song, B. Bob, Y. Yang, *Phys. Chem. Chem. Phys.* **2014**, *17*, 112.
[91] S. D. Stranks, V. M. Burlakov, T. Leijtens, J. M. Ball, A. Goriely, H. J. Snaith, *Phys. Rev. Appl.* **2014**, *2*, 1.
[92] W.-J. Yin, T. Shi, Y. Yan, *Appl. Phys. Lett.* **2014**, *104*, 063903/1.
[93] J. Kim, S. Lee, J. H. Lee, K. Hong, *J. Phys. Chem. Lett.*, **2014**, *5*, 1312.
[94] T. Leitgens, G. Eperon, A. Barker, G. Grancini, W. Zhang, J. Ball, A. R. Srimath Kandada, H. Snaith, A. Petrozza, *Energy Environ. Sci.* **2016**, *9*, 3472.
[95] J. S. Yun, A. Ho-Baillie, S. Huang, S. H. Woo, Y. Heo, J. Seidel, F. Huang, Y. B. Cheng, M. A. Green, *J. Phys. Chem. Lett.* **2015**, *6*, 875.
[96] E. Edri, S. Kirmayer, S. Mukhopadhyay, K. Gartsman, G. Hodes, D. Cahen, *Nat. Commun.* **2014**, *5*, 3461.

[97] A. Abate, M. Saliba, D. J. Hollman, S. D. Stranks, R. Avolio, A. Petrozza, J. Snaith, *Nano Lett.* **2014**, *14*, 3247.
[98] N. K. Noel, A. Abate, S. D. Stranks, E. S. Parrott, V. M. Burlakov, A. Goriely, H. J. Snaith, *ACS Nano* **2014**, *8*, 9815.
[99] Y. Shao, Z. Xiao, C. Bi, Y. Yuan, J. Huang, *Nat. Commun.* **2014**, *5*, 1.
[100] Q. Dong, Y. Yuan, Y. Shao, Y. Fang, Q. Wang, J. Huang, *Energy Environ. Sci.* **2015**, *8*, 2464.
[101] W. Nie, H. Tsai, R. Asadpour, J.-C. Blancon, A. J. Neukirch, G. Gupta, J. J. Crochet, M. Chhowalla, S. Tretiak, M. A. Alam, H.-L. Wang, A. D. Mohite, *Science* **2015**, *347*, 522.
[102] C. Bi, Q. Wang, Y. Shao, Y. Yuan, Z. Xiao, J. Huang, *Nat. Commun.* **2015**, *6*, 7747.
[103] W. Li, H. Dong, L. Wang, N. Li, X. Guo, J. Li, Y. Qiu, *J. Mater. Chem. A* **2014**, *2*, 13587.
[104] H. J. Snaith, A. Abate, J. M. Ball, G. E. Eperon, T. Leijtens, N. K. Noel, S. D. Stranks, J. T. W. Wang, K. Wojciechowski, W. Zhang, *J. Phys. Chem. Lett.* **2014**, *5*, 1511.
[105] H. Kim, K.-G. Lim, T.-W. Lee, *Energy Environ. Sci.* **2016**, *9*, 12.
[106] P. W. Liang, C. C. Chueh, S. T. Williams, A. K. Y. Jen, *Adv. Energy Mater.* **2015**, *5*, 1.
[107] L. Zuo, Z. Gu, T. Ye, W. Fu, G. Wu, H. Li, H. Chen, *J. Am. Chem. Soc.* **2015**, *137*, 2674.
[108] V. Adinolfi, M. Yuan, R. Comin, E. S. Thibau, D. Shi, M. I. Saidaminov, P. Kanjanaboos, D. Kopilovic, S. Hoogland, Z.-H. Lu, O. M. Bakr, E. H. Sargent, *Adv. Mater.* **2016**, *28*, 3406.
[109] A. Mei, X. Li, L. Liu, Z. Ku, T. Liu, Y. Rong, M. Xu, M. Hu, J. Chen, Y. Yang, M. Grätzel, H. Han, *Science* **2014**, *345*, 295.
[110] M. Burgelman, P. Nollet, S. Degrave, *Thin Solid Films* **2000**, *361-362*, 527.
[111] H. J. Snaith, *J. Phys. Chem. Lett.* **2013**, *4*, 3623.
[112] C. C. Stoumpos, C. D. Malliakas, M. G. Kanatzidis, *Inorg. Chem.* **2013**, *52*, 9019.
[113] A. Kanevce, W. K. Metzger, *J. Appl. Phys.* **2009**, *105*, 94507.
[114] Y. Liu, Y. Sun, W. Liu, J. Yao, *Phys. Chem. Chem. Phys.* **2014**, *16*, 15400.
[115] V. Q. Dang, G.-S. Han, T. Q. Trung, L. T. Duy, Y.-U. Jin, B.-U. Hwang, H.-S. Jung, N.-E. Lee, *Carbon* **2016**, *105*, 353.
[116] Y. Lee, J. Kwon, E. Hwang, C.-H. Ra, W. J. Yoo, J.-H. Ahn, J. H. Park, J. H. Cho, *Adv. Mater.* **2014**, *27*, 41.
[117] Y. Fang, J. Huang, *Adv. Mater.* **2015**, *27*, 2804.
[118] Y. Guo, C. Liu, H. Tanaka, E. Nakamura, *J. Phys. Chem. Lett.* **2015**, *6*, 535.
[119] X. Hu, X. Zhang, L. Liang, J. Bao, S. Li, W. Yang, Y. Xie, *Adv. Funct. Mater.* **2014**, *24*, 7373.
[120] M. I. Saidaminov, M. A. Haque, M. Savoie, A. L. Abdelhady, N. Cho, I. Dursun, U. Buttner, E. Alarousu, T. Wu, O. M. Bakr, *Adv. Mater.* **2016**, *28*, 8144.
[121] Z.-K. Tan, R. S. Moghaddam, M. L. Lai, P. Docampo, R. Higler, F. Deschler, M. Price, A. Sadhanala, L. M. Pazos, D. Credgington, F. Hanusch, T. Bein, H. J. Snaith, R. H. Friend, *Nat. Nanotechnol.* **2014**, *9*, 687.
[122] G. Li, Z.-K. Tan, D. Di, M. L. Lai, L. Jiang, J. H.-W. Lim, R. H. Friend, N. C. Greenham, *Nano Lett.* **2015**, *15*, 2640.
[123] A. Miyata, A. Mitioglu, P. Plochocka, O. Portugall, J. T.-W. Wang, S. D. Stranks, H. J. Snaith, R. J. Nicholas, *Nat. Phys.* **2015**, *11*, 582.
[124] M. E. Ziffer, J. C. Mohammed, D. S. Ginger, *ACS Photonics* **2016**, *3*, 1060.
[125] V. D'Innocenzo, G. Grancini, M. J. P. Alcocer, A. R. S. Kandada, S. D. Stranks, M. M. Lee, G. Lanzani, H. J. Snaith, A. Petrozza, *Nat. Commun.* **2014**, *5*, 3586.
[126] G. Grancini, A. R. Srimath Kandada, J. M. Frost, A. J. Barker, M. De Bastiani, M. Gandini, S. Marras, G. Lanzani, A. Walsh, A. Petrozza, *Nat Photonics* **2015**, *9*, 695.
[127] Y. Yang, M. Yang, Z. Li, R. Crisp, K. Zhu, M. C. Beard, *J. Phys. Chem. Lett.* **2015**, *6*, 4688.
[128] J. A. Sichert, Y. Tong, N. Mutz, M. Vollmer, S. Fischer, K. Z. Milowska, R. García Cortadella, B. Nickel, C. Cardenas-Daw, J. K. Stolarczyk, A. S. Urban, J. Feldmann, *Nano Lett.* **2015**, *15*, 6521.
[129] J. S. Manser, P. V. Kamat, *Nat. Photonics* **2014**, *8*, 737.

